Journal of Materiomics 12 (2026) 101206

Contents lists available at ScienceDirect

Journal of Materiomics

journal homepage: www.journals.elsevier.com/journal-of-materiomics/

Spatially resolved performance evaluation of next-generation electrocatalyst support assemblies for water electrolyzers

Soma J. Keszei [a], Tímea Benkó [b], Sahir A.M. Al-Zuraiji [b], Dimitris Niarchos [c], Levente Tapasztó [a], József S. Pap [b,*]

[a] HUN-REN Centre for Energy Research, Institute of Technical Physics and Materials Science, Konkoly-Thege M. Street 29-33, 1121, Budapest, Hungary
[b] HUN-REN Centre for Energy Research, Department of Surface Chemistry and Catalysis, Konkoly-Thege M. Street 29-33, 1121, Budapest, Hungary
[c] AMEN New Technologies IKE, Mesogeion 553, Aghia Paraskevi, Attikis 15343, Athens, Greece

ARTICLE INFO

Article history:
Received 21 November 2025
Received in revised form
19 January 2026
Accepted 28 January 2026
Available online 12 March 2026

Current (photo)electrolysis for solar hydrogen generation is limited by its dependence on noble- or less abundant transition metal catalysts. Proton exchange membrane (PEM) water electrolysis is highly suitable for coupling with intermittent renewables like solar power due to its high power density and load-following capability [1]. A critical drawback is the reliance on iridium-based oxides as the anode catalyst for the oxygen evolution reaction (OER). Despite their unmatched stability under harsh acidic conditions, the global supply of iridium is severely limited (7–8 t per year). Current catalyst loadings (2–4 $mg_{Ir} \cdot cm^{-2}$) restrict the maximum annual PEM electrolyzer installation capacity to approximately 10 GW [2]. Two fundamental strategies address this issue by pursuing next-generation electrocatalysts: (1) metal dilution/structural engineering to maintain performance with less iridium, and (2) exploring catalysts based on abundant elements. Both strategies necessitate truly atom-efficient catalyst synthesis — at minimized concentrations in the case of iridium — and require maximizing the contribution of the catalytic sites in order to meet the performance needs. The synthesis of such systems also involves support materials, which the catalysts are grafted onto at the atomic-to-nano-scale. Despite high-precision synthesis methods, diverse active site structures can exist within these complex systems, as structural uniformity is heavily influenced by catalyst–support interactions and the specific conditions of synthesis and operation. Due to the above complexities, catalysts should be assumed to be structurally non-uniform until shown otherwise, as postulated by Bates [3].

An efficient catalyst synthesis must correlate fabrication parameters with the resulting structural distribution, prioritizing the controllable creation of highly active sites that are identifiable. Consequently, traditional bulk electrochemical benchmarking, which averages catalyst performance often leading to empirically optimized catalyst loads may be insufficient. This perspective highlights the potential and limitations of scanning electrochemical cell microscopy (SECCM) as a contemporary technique for studying catalysts at high spatial resolution, providing insights into the correlation of chemical and structural information with catalytic activity and mechanisms.

1. Benchmarking methodology for anode catalysts

Establishing and applying standardized protocols for assessing OER catalyst performance and durability remains a primary challenge, often leading to discrepancies in how experimental results are interpreted [4]. Note that benchmarking procedures for heterogeneous OER catalysts have been proposed under conditions relevant to an integrated solar water-splitting device [5]. The most generally applied tests are shown in Fig. 1.

Chronopotentiometry (CP) or -amperometry (CA) that are meant to simulate steady operating conditions of PEMWEs. CP gives a durability descriptor as the change in cell potential in the function of time (mV/h). CA measures the change in the current density in similar terms (mA/h). The accelerated stress test (AST)

This article is part of a special issue entitled: 10th anniversary published in Journal of Materiomics.

* Corresponding author.
E-mail address: pap.jozsef@ek.hun-ren.hu (J.S. Pap).

https://doi.org/10.1016/j.jmat.2026.101206

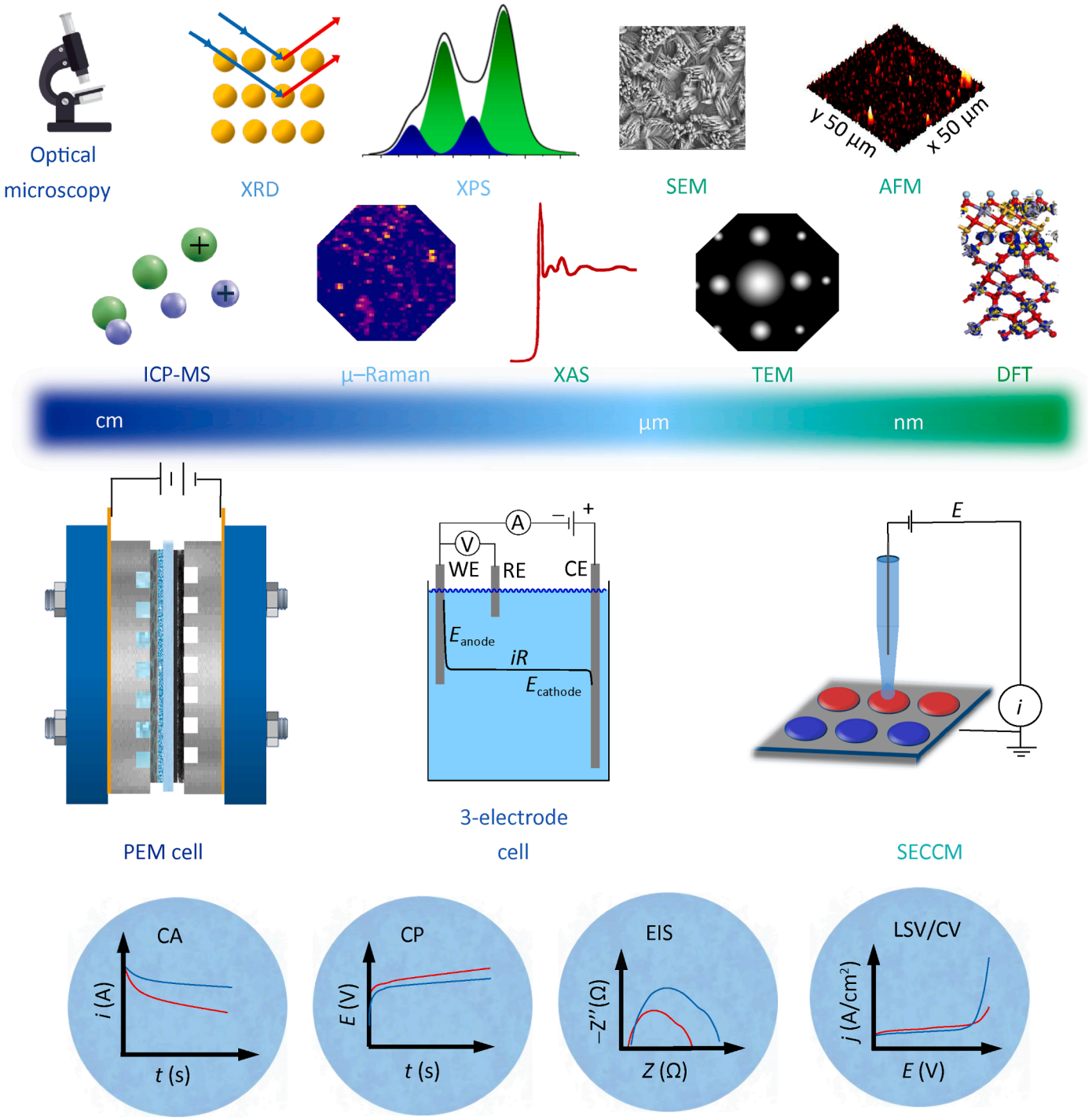

Fig. 1. Multi-scale physicochemical characterization with a library of analytical techniques and electrochemical benchmarking of catalyst layers.

by means of potential cycling (cyclic voltammetry, *i.e.*, CV) in a defined potential range on the other hand simulates the frequent starting and shutdown under intermittent operation. Electrochemical impedance spectroscopy (EIS) can decouple the complex physical and chemical processes occurring simultaneously within the cell as a whole and allow elucidating exactly which component is limiting performance. Equivalent circuit models (ECMs) help breaking down components to ohmic resistance (R_S) representing the resistance of the membrane, ionomer, and electrical contacts (porous transport layer (PTL)/bipolar plates), to charge transfer resistance (R_{ct}) reflecting the kinetics of the OER, and mass transport resistance (R_{mt}) representing mass transport difficulties (for example, moving water to the catalyst or removing oxygen bubbles from the electrode). In durability studies, EIS is used as a 'health check' during and after AST. By comparing the EIS over time an increase in R_S may indicate membrane thinning, dehydration, the oxidation of the PTL or the accumulation of impurities. An increase in R_{ct} indicates catalyst dissolution/agglomeration by a loss of electrochemically active surface area (ECSA) or the degradation of the catalyst. Lastly, catalysts are often benchmarked *via*

Tafel analysis, the fundamental method for evaluating OER kinetics by determining the activation overpotential (η) and the exchange current density (j_0, representing the intrinsic activity at equilibrium). Tafel analysis is typically performed using CA at discrete potential steps or slow-scan LSV in a three-electrode cell. In these settings, *i*R-compensation, the mitigation of mass transport effects, and precise linear-region selection are critical for accuracy. In a PEMWE setup, the focus shifts from material characterization to device testing, where these interfacial effects often become dominant. Nevertheless, rigorously applied Tafel analysis remains useful for decoupling kinetic overpotential from ohmic resistance, facilitating mass activity comparisons, and benchmarking loading effects to determine whether reduced catalyst loading alters the reaction mechanism or simply diminishes the number of available active sites.

Additional derived parameters also provide a useful basis for data comparison. Kim et al. reported the use of a so-called activity-stability factor (ASF) to evaluate the balance between the OER activity and stability of an $Ir_{25}Os_{75}$ alloy electrocatalyst [6]. They proposed the ASF as the ratio between the rate of oxygen production (current density, J) and the rate of metal dissolution (equivalent dissolution current density, S) at a specific overpotential, ASF = $(J-S)/S$. Electrocatalysts with higher ASF possess higher durability. Similarly, Geiger and Cherevko et al. introduced the stability number (S-number) to explore the dissolution behavior of Ir-based oxides [7]. The S-number is defined as the ratio between the number of produced oxygen molecules and the dissolved iridium atoms and hence is independent of involved active sites (the same as the ASF in principle). The larger the S-number, the more superior the stability of the electrocatalysts. However, both methods require online ICP-MS apparatus to detect *in situ* oxygen molecules and dissolved iridium ions. Both the ASF and the S-number regard the dissolution of catalyst as the sole factor for the degradation, but other irreversible structure changes such as catalyst poisoning, agglomeration and lattice collapse during the OER would also contribute to the failure of electrocatalysts and hence post-OER characterizations play an important role in evaluating the catalyst stability and in revealing the corresponding structure-function relation.

Experimental configuration is another critical factor in the interpretation of electrochemical data. Catalysts are often initially screened in three-electrode or dual-compartment H-cells before being integrated into full MEAs for PEMWE device-level testing. However, conditions differ significantly between these setups. While PEMWE systems operate with pure water at elevated pressures and temperatures under flow, the acidity in the anode catalyst layer is often overestimated in H-cells using liquid electrolytes like 0.5 mol/L H_2SO_4 and 0.1 mol/L $HClO_4$ compared to MEAs and all of these can directly impact catalyst behavior. For example, IrO_x can be stabilized by anodic-current-induced crystallization. Thus, the higher current densities typical of MEA conditions can lead to faster stabilization than that observed in H-cells.

Furthermore, efficient catalysis requires a three-phase boundary (TPB), where the catalyst maintains simultaneous contact with the electron conductor, the electrolyte, and the escaping product gas. A bridging option between H-cells and PEMWEs is the gas diffusion electrode (GDE) cell, which facilitates a more straightforward creation of the TPB. Physical dimensions also influence performance requirements. While high support conductivity may be less critical in an H-cell, it becomes indispensable in a real MEA system, where the catalyst layer thickness is approximately 10 μm. Additionally, while strong metal-support interactions (SMSI) are crucial for ensuring structural uniformity, these interactions can be modified by the presence of ionomers in MEA catalyst inks. The upscaling process itself — including catalyst ink preparation, spray coating, and hot pressing into large-area MEAs — can compromise the representative nature of results obtained from small-scale analysis. In practice, the uniformity of the catalyst layer thickness and the evenness of mechanical pressure in the stack fundamentally control the proportion of the effective catalyst amount, adding complexity to the successful transfer of laboratory findings. Ultimately, establishing a protocol that ensures comparable and relevant data interpretation is a multifaceted challenge. The following section examines the necessity of spatially resolved performance evaluations for the OER, highlighted through contemporary examples across various catalytic systems.

2. Recent anode catalyst developments

A key study reported an atomically dispersed hexavalent iridium oxide Ir^{VI} derived from MnO_2 reduction (Ir^{VI}-ado), achieving an initial mass-specific current density of 5×10^4 $A \cdot g_{Ir}^{-1}$ [2]. Optimization (using a Pt-coated sintered Ti-powder support, thicker Nafion 212, and thinner MnO_2) increased activity to over 1.7×10^5 $A \cdot g_{Ir}^{-1}$ at 1.75 V, corresponding to 7 A/cm^2 at a remarkably low loading of 0.08 $mg_{Ir} \cdot cm^{-2}$. This resulted in a TOF of 83 s^{-1} per Ir atom and a projected annual installation capacity exceeding 324 GW. Excellent stability was confirmed, with long-term testing exceeding 2700 h and a low degradation rate of −6.5 μV/h. *In-situ* X-ray Absorption Spectroscopy (XAS) confirmed Ir^{VI} as the dominant species, and EXAFS showed short Ir–O bonds and Ir–O–Mn coordination. Additional characterization by scanning electron microscopy (SEM) and energy-dispersive X-ray (EDX) verified the presence of a few-micron thin manganese oxide layer containing highly dispersed Ir over the titanium support. The authors noted that degradation increased upon lowering Ir loadings, suggesting that factors beyond atom dispersion influence individual Ir atom contribution to the overall performance.

Mesoporous antimony tin oxide (ATO) with a particle assembly structure proved efficient in stabilizing IrO_2 (IrO_2/ATO) [8]. In a PEM electrolyzer (Nafion 212), IrO_2/ATO achieved a current density of 2 A/cm^2 at 1.8 V with a low loading of 0.3 $mg_{Ir} \cdot cm^{-2}$, showing outstanding stability at 1 A/cm^2 and 80 °C. The high OER performance was attributed to a strong metal oxide-support interaction (SMOSI), confirmed by structural analysis and density functional theory (DFT). The SMOSI reduced the overpotential to 272 mV at 10 mA/cm^2 and increased the mass-specific activity to over 175 $A \cdot g_{Ir}^{-1}$ in a three-electrode setup. Material superiority was explained by an increased specific surface area (promoting IrO_2 dispersion and creating ATO-IrO_2 interfacial active sites), facilitated mass transfer by the 2–5 nm mesopores, and enhanced electrical conductivity. Detailed characterization by XPS and XAS indicated Ir^{IV} on the surface in 84.3%, confirming an electronic structure modification of IrO_2 by the ATO support. Raman spectroscopy implied an Ir–O–Sn phase. Structural analysis by TEM/HAADF-STEM/XRD confirmed uniform Ir distribution and aggregate-derived large pores (20–100 nm). Yet, a gap remains between dimensions and scope, as structural/valence-state analyses provide averaged characteristics across all Ir sites, while DFT models a specific, sub-nanometer scale cell, implying that the averaged metrics may mask atomistic performance differences.

Shape-controlled, mass transport enhanced Ir nanodendrites supported on ATO nanoparticles (MTE IrND/ATO) were reported [9]. Detailed TEM analysis showed an Ir domain size of 1.7 nm and a particle size of 11.2 nm being smaller compared to conventional nanodendrites. XPS determined the surface Ir species distribution to be 47% Ir^0, 36% Ir^{IV} and 18% Ir^{III}. Kinetic and transport overpotentials were elucidated as a function of current density in a PEM single cell (Nafion 212, 80 °C). The shape-controlled structure

resulted in a 10% decreased transport overpotential at 3 A/cm^2 compared to conventional nanodendrites. The MTE IrND/ATO demonstrated high stability, with a low degradation rate (~83 μV/h) over 280 h at 2 A/cm^2. While the benefit of shape control was clearly benchmarked against other Ir nanostructures, the specific contribution of the various ATO-nanodendrite contact assemblies to the overall performance remains unexplored.

To counter issues like catalyst detachment and low active site availability arising from MEA preparation using ionomers, an effective strategy is the fabrication of self-supported electrodes on a Ti-mesh. A prominent example is nitrogen-doped TiO_2 nanotube arrays (N-TNTAs) activated with electrodeposited IrO_2 (IrO_2/N-TNTA) [10]. This configuration improves mass-specific activity (reaching 431.2 A· $g_{IrO_2}{}^{-1}$) and stability at a loading of 27.88 μg·cm^{-2} (based on ICP–OES). The enhancement is attributed to improved active site availability and favorable electronic interactions from nitrogen doping, which also enhances conductivity to 60% of the pristine Ti-mesh. Specifically, the N-TNTAs (50–100 nm diameter) increase the Ir^{III}-content (statistically 65% *via* XPS) and oxygen vacancies, thus boosting activity. The ordered structure enhances mass transfer kinetics and facilitates uniform IrO_2 dispersion. While statistical characterization supports these conclusions, spatially resolved analysis would be valuable to determine the specific contribution of potentially differing catalyst-support surface assemblies.

Despite stabilization efforts, time- and potential-resolved electrochemical dissolution profiles established that Ir can dissolve below the OER onset due to transient surface oxidation and reduction. Whether the reaction proceeds *via* the adsorbate evolution mechanism (AEM) or the lattice oxygen-mediated mechanism (LOM) [11] dictates the specific dissolution pathway involved. Consequently, it remains an intriguing question, how these processes manifest at diverse nanoscale localities within the complex matrix of a MEA ink.

Beyond Ir, transition metal oxides (TMOs) are gaining attention as catalyst-support systems. TMOs are typically favored in alkaline water electrolyzers (AELs), which are economically competitive for large, constant-load applications but struggle with fluctuating renewable power, although new cell designs (like capillary-fed cells) may change this landscape [12]. This design has demonstrated 1.5 V at 0.5 A/cm^2 and 98% energy efficiency (higher heating value, HHV) [12]. For abundant TMO-based systems, the key challenges remain the reduction of the intrinsically high overpotentials, the increase of current densities by tuning the electronic structure of catalysts and the improvement of durability. Overcoming issues of inadequate conductivity and restricted accessibility of active sites are also existing problems. Cobalt oxide is an emblematic OER catalyst, often forming Co_3O_4 *in situ* across various supports. A recent study demonstrated that support modification coupled with lattice defects is a viable strategy to enhance stability and reduce overpotential under acidic conditions. Bi and Ni co-doped Co_3O_4 phase on carbon paper (BiNi–Co_3O_4/CP) achieved an overpotential of 275 mV and demonstrated stability for 110 h at 10 mA/cm^2 [13]. Bismuth induces lattice expansion in spinel-type nanosheets, creating highly reactive interfaces, and etches the carbon paper support to enhance porosity. Nickel, conversely, controls porosity by inhibiting Co_2C formation. While solid evidence supports the enhanced OER properties, the lack of reported PEM single cell results leaves the question of practical benefits in a complex environment open.

Atomic dispersion of metal catalysts is an effective strategy to manipulate intrinsic activity. A complex nanomaterial, a-Ni/CeO_2@NC (atomically dispersed Ni anchored on CeO_2 particles entrenched on peanut-shaped hollow nitrogen-doped carbon) benefits from adjacent Ce sites to Ni to enhance OER performance [14]. The overpotential is merely 286 mV at 10 mA/cm^2. Exhaustive characterization confirmed the unique structure of these uniform, hollow nanoparticles, resulting in a TOF of 4 s^{-1}, and stability exceeding 100 h at 10 mA/cm^2. The catalyst was benchmarked against isomorphous a-Ni@NC, CeO_2@NC and RuO_2 in 1 mol/L KOH, each dispersed over carbon paper by the ink method using Nafion. Despite the meticulous characterization and the uniformity of the catalyst, one might wonder whether the distribution of catalytic performance is equally uniform across the material.

The study of high entropy oxide (HEO) nano-catalysts is also highly relevant. For example, the spinel-type $(FeCoNiCrMn)_3O_4$ was reported as highly efficient OER catalyst under alkaline conditions, drop-casted with Nafion onto a carbon cloth [15]. It achieved a remarkable 239 mV overpotential at 10 mA/cm^2 and maintained stability for over 24 h at 100 mA/cm^2. *In situ* Raman spectroscopy identified active MOOH surface species and dynamic changes in M−O stretching bands at anodic potentials. The superior performance of $(FeCoNiCrMn)_3O_4$ is attributed to the synergism among the randomly mixed metal cations, which are dynamically formed *in situ*, and the high entropy effect maintaining the spinel structure. Note that the stabilizing effect of configurational entropy in HEOs is often misunderstood or oversimplified. In a spinel lattice such as $(FeCoNiCrMn)_3O_4$, multiple cations share the tetrahedral and octahedral sites in a near-random distribution. Each cation has different preferred coordination geometries, ionic radii, and oxidation states, and in a conventional mixed-oxide this chemical diversity would lead to phase segregation or the formation of multiple oxide domains. However, at certain mixing levels, the configurational entropy becomes large enough to offset the enthalpic penalty of disorder. The entropy term lowers the Gibbs free energy and stabilizes a homogeneous phase, even if the enthalpy of mixing is locally unfavorable. The result is a robust spinel oxide in which the cationic sub-lattices contain a statistical distribution of local environments, each potentially exhibiting distinct redox behavior and catalytic properties. While the advantages of HEOs are clear, further insight into the structure-reactivity relationships at a sub-micron scale remains a fascinating possibility.

Lastly, molecular OER catalysts based on first-row transition metal complexes may also hold promise in their integration — foremost, but not exclusively — into photoelectrocatalytic (PEC) systems *via* surface grafting. Electrochemistry remains the main technique that allows for the proper evaluation of catalytic activities, in combination with spectroscopy and microscopy, which help to characterize the whole system [16] as also illustrated in Fig. 1. Operando stability and dynamics of complexes on (photo)-electrode surfaces is an intrinsic problem that calls for advanced electrochemical techniques like SECCM.

3. Perspectives on scanning electrochemical cell microscopy

SECCM is an emerging technique that offers insights into the nanoscale heterogeneity of surfaces, enabling correlation between surface features and electrochemical activity [17]. The method constitutes a powerful means of probing dynamics of interfaces, where changes in local ion adsorption/desorption/exchange, dissolution and growth take place, among other possibilities. Localized amperometric mapping of heterogeneously active electrode surfaces is readily realized with SECCM. Utilizing a mobile nano-droplet cell, SECCM scans surfaces with high spatial resolution, generating electrochemical maps (alongside topographical information in certain operating modes). The unmatched advantage of SECCM is its applicability on diverse samples, such as nanoparticles, polymers, 2D materials, thin-layers and polycrystalline substrates, thereby elucidating individual contributions

to catalysis [18]. The method relies on a nano-pipette probe containing the electrolyte and a quasi-reference counter electrode (QRCE). The electrochemical cell is established when the electrolyte meniscus contacts the substrate surface. The scanning mode allows CA, while the probe moves across the surface, whereas the hopping mode uses an approach-retract cycle to generate distinct measurement points, allowing for detailed LSV or CV analyses (*e.g.*, Tafel plots). Importantly, it has a well-defined droplet size, which cannot be assured in scanning mode. The spatial resolution is governed by the nano-pipette aperture and the degree of surface wetting. While early studies relied exclusively on nano-pipettes fabricated by laser-based micropipette puller creating custom aperture sizes, standardized pipettes with opening diameters of 100 nm and 500 nm have become commercially available recently, improving experimental reproducibility. Electrolyte footprints left on the surface permit accurate calculation of current densities [19], and the same measured area can be post-characterized using techniques like SEM, AFM, and XPS.

SECCM facilitates the direct establishment of structure-activity relationships [20], especially on smooth, 2D catalyst surfaces [21]. Tsujiguchi *et al*. employed SECCM to investigate the CO_2 reduction reaction (CO_2RR) on a composite of Sn nanoparticles (15–50 nm) supported on reduced graphene oxide (rGO) [22]. By mapping the local activity, they identified distinct electrochemical zones, of which the Sn/rGO boundary exhibited a sevenfold increase in current density, pinpointing it as the primary catalytic site. These findings suggest that CO_2RR performance can be maximized by optimizing Sn loading, specifically by reducing nanoparticle diameter or ensuring a dense distribution of discrete particles to maximize the density of exposed interfacial sites.

Visualization of active sites on MoS_2 nanosheets for the hydrogen evolution reaction (HER) on highly oriented pyrolytic graphite (HOPG) support could be also achieved [23]. Using a 20 nm radius nanopipette (0.5 mol/L H_2SO_4 electrolyte) local overpotentials at 30 mA/cm^2 was mapped. Tafel slopes with submicron resolution helped identifying high-activity nanosheet edges, terraces, and grain boundaries, directly correlating the local morphology of MoS_2 with its electrochemical efficiency. Mefford et al. utilized correlative operando SECCM combined with X-ray microscopy to resolve the bulk structural changes that drive surface activity in OER catalysis. By high-resolution electrochemical mapping on single-crystalline β-$Co(OH)_2$ platelets, the intrinsic activity of specific facets revealed that the catalytic behavior is directly correlated with the local concentration of Co^{3+} at reactive edge sites [24]. By leveraging the high spatial resolution of the meniscus-based probe, single-entity activity mapping could be performed both between different hematite nanorods and within a single rod over HOPG [25]. SECCM resolved the intrinsic electrocatalytic heterogeneity of individual nanorods during the OER. A significant intra-entity performance gradient could be revealed from the body to the tip attributed to the larger fraction of exposed {001} active facets on the body.

Although SECCM offers spatially resolved high throughput measurements on versatile substrates, the technique faces challenges, regarding droplet stability, as evaporation and uncontrolled surface wetting can alter electrolyte concentrations or spatial precision. Furthermore, when moving the probe small amounts of electrolyte are left behind on the surface, which can cause 'cross-talk' between adjacent measurement sites. The resolution depends heavily on the droplet size and stability. Robust experiments with higher resolution can be achieved by silanizing the outer surface of the glass capillary, incorporating electrolyte additives, or coating the sample with a thin hydrophobic oil layer. In addition, complex instrumentation and ultra-sensitive feedback systems make the experiments susceptible to mechanical noise.

The capabilities of SECCM are compromised by porous, or powdered samples, like the OER catalyst-support assemblies or MEA inks. However, thinned, pore-free catalyst-support ink layers may be suitable for analysis. The thickness of anode catalyst layers pressurized between the PTL and the ionomer membrane in PEMWE cells reach 10 μm (Fig. 2a). On standard conductive substrates like ITO, or FTO glass (also suitable for correlative analyses using navigational aids) spin-coated quasi-2D ink layers can be prepared, corresponding to a few overlaid nanoparticles at square centimeter areas (Fig. 2b). On the thinned specimens bulk and localized analysis is done in a reproducible manner and electrochemical features can be directly compared, for example LSVs (Fig. 2c). The high spatial resolution allows for identifying diversities in activity, and selected spots can be further analyzed by several methods to identify structure-activity correlations and bottlenecking factors (Fig. 2d). The structural and compositional complexities in large-area MEAs highly justify such efforts as implicit performance reserves often remain unexplored. Achieving true homogeneity across MEAs would mean ensuring uniform nanoparticle dispersion, balanced mass transport, identical ohmic losses, and uniform catalytic performance across individual active sites that are particularly ambiguous given the complexity of the systems. Beyond collecting bulk parameters that describe the average total surface area, this approach may distinguish contribution of individual or well-defined groups of catalytic centers to the overall activity, thereby providing statistics on heterogeneity.

Fig. 2e shows the adaptation of the above strategy to a reported molecular OER catalyst, FePBI, where PBI is 2-(2′-pyridyl)benzimidazole [26]. FePBI has been previously investigated in both homogeneous solution and heterogenized on an ITO electrode as a self-supported layer. The electron-donating NH-group in PBI allows the complex to access and support higher oxidation states, rendering it stable during catalysis. We utilized FePBI and ATO as a support (Thermo Fisher, NanoArc, 21 nm average particle size) mixed with Nafion. The complex is readily grafted onto ATO from isopropanol through ligand exchange and is expected to provide different surface formations based on its solution chemistry [26]. The electrochemical behavior of the FePBI/ATO/Nafion system was explored on spin-coated thin layers over ITO as the working electrode in SECCM (ParkSystems NX10, SECCM/AFM instrument). Surface imaging by optical microscopy confirmed a continuous thin layer with an average thickness of 248 nm and RMS factor (S_q) of 79 nm from AFM (Fig. 2e). AFM was complemented with Raman microscopy, a powerful tool used to simultaneously detect characteristic vibration bands from the ATO support and the PBI ligand coordinated to Fe revealed satisfactory FePBI coverage over ATO. SECCM was then performed in the hopping mode over a 50 μm× 50 μm area, collecting LSV from 100 droplets at nominal tip opening diameter of 500 nm (Fig. 2e). Stabilizing the actual contact area was a major challenge: it is not necessarily identical to the capillary aperture, as surface wetting properties vary depending on the sample. In this case, the conversion from current-to-current density was achieved by using optical microscopy to measure the footprints left by the electrolyte droplets (approximately 2 μm^2 each, Fig. 2e). The resulting current maxima at 1.6 V *vs.* Ag/AgCl QRCE were converted to a color map in yellow to blue to visualize heterogeneities. A histogram of the occurrence frequency for the Faraday currents at 1.6 V revealed two well-distinguished groups of LSVs. A smaller group produced lower currents, indicating a modestly active FePBI-ATO assembly, whereas a larger group produced markedly higher Faraday currents, indicating the presence of a more active FePBI-ATO assembly. These significant differences that appoint the spots of post-catalytic analysts remain hidden when LSV is performed over the entire area (Fig. 2c, grey curve).

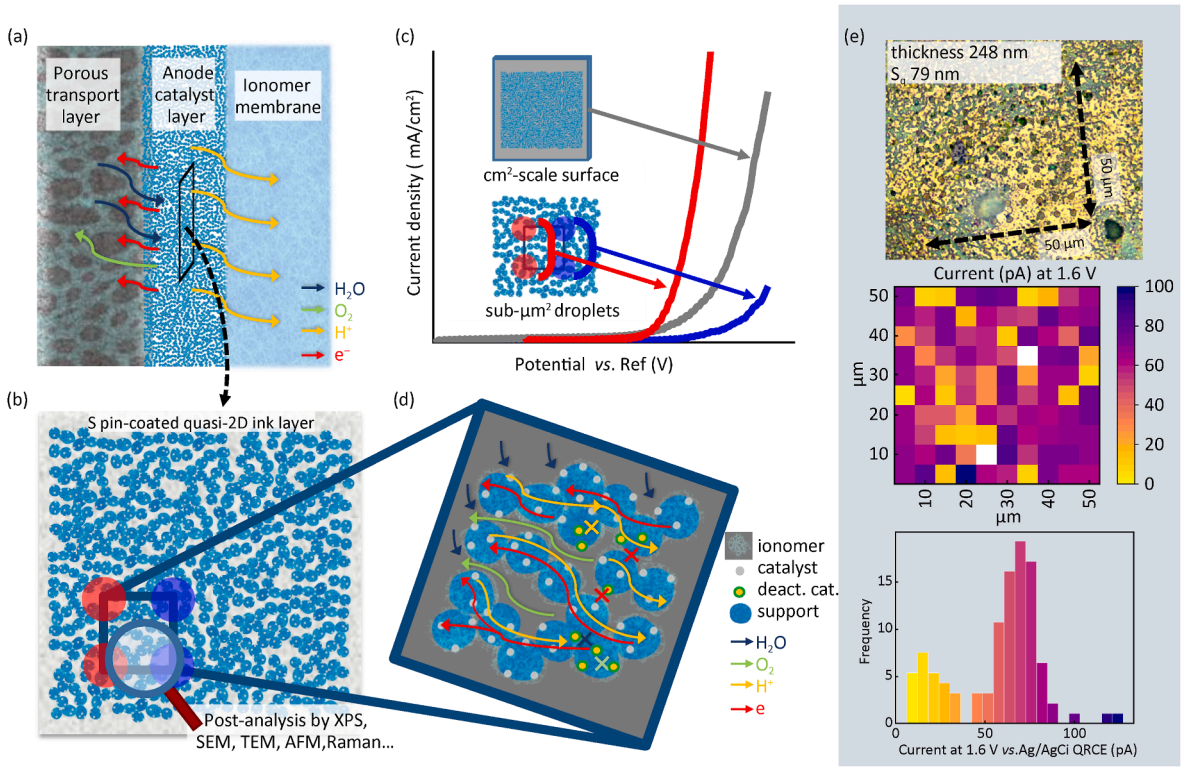

Fig. 2. (a) Anode catalyst layer (CL) in between the PTL and ionomer membrane with transport directions in a PEMWE assembly; (b) spin-coated thin layer of the catalyst-support assemblies identical to the composition of the CL (red and blue circles represent spots of SECCM analysis); (c) LSVs recorded at the overall surface and the color coded spots of the thin CL; (d) relevant transport processes and catalyst distribution in a magnified area of the thin CL suitable for correlative studies; (d) optical microscopy image of a thin FePBI/ATO/Nafion ink (CL) over FTO with footprints of SECCM analysis, the corresponding square-map of lateral activities representing individual LSV experiments (1 V/s, 0.1 mol/L $NaClO_4$, current at 1.6 V *vs.* Ag/AgCl QRCE); histogram of Faradaic currents in SECCM.

4. Conclusions and outlook

The overall performance of OER catalyst-support assemblies in complex environments like MEAs is a manifold question. While modern bulk evaluation techniques are practically valid, the true contributions from different catalyst-substrate arrangements require advanced, spatially resolved techniques, like SECCM that provides a vital complement to traditional methods (*e.g.*, electrochemical impedance spectroscopy, Tafel analysis, stability testing) by enabling visualization and weighting of relative contributions across the assembly. Rational catalyst design must shift from optimizing only the most active bulk catalyst-support combination to enriching the most active site variations identified through spatially resolved analysis. Note that similar considerations apply to integrated systems, where nanoscale noble- or transition metal-based co-catalysts are combined with semiconductor surfaces. Utilizing SECCM expedites the optimization of synthesis parameters, thus accelerating the fabrication of better MEAs and/or photoanodes.

CRediT authorship contribution statement

Soma J. Keszei: Writing – original draft, Visualization, Methodology, Investigation, Formal analysis, Data curation. **Tímea Benkó:** Writing – original draft, Investigation, Formal analysis. **Sahir A.M. Al-Zuraiji:** Methodology, Investigation, Data curation. **Dimitris Niarchos:** Writing – review & editing, Writing – original draft. **Levente Tapasztó:** Writing – review & editing, Supervision, Resources, Methodology, Funding acquisition. **József S. Pap:** Writing – review & editing, Writing – original draft, Supervision, Methodology, Funding acquisition, Conceptualization.

Declaration of competing interest

The authors declare that they have no known competing financial interests or personal relationships that could have appeared to influence the work reported in this paper.

Acknowledgements

The authors thank the National Laboratory for Renewable Energy (Hungary) for support, financed by the RRF-2.3.1-21-2022-00009 project, and the European Union's Horizon Europe research and innovation programme HORIZON-MSCA-2023-SE-01 under grant agreement No 101183082 – PacemCAT, and Élvonal (Forefront) grant KKP 138144.

References

[1] Wang CR, Stansberry JM, Mukundan R, Chang H-MJ, Kulkarni D, Park AM, et al. Proton exchange membrane (PEM) water electrolysis: Cell-level considerations for gigawatt-scale deployment. Chem Rev 2025;125:1257–302.
[2] Li A, Kong S, Adachi K, Ooka H, Fushimi K, Jiang Q, et al. Atomically dispersed hexavalent iridium oxide from MnO_2 reduction for oxygen evolution catalysis. Science 2024;384:666–70.
[3] Bates JS. Progress and pitfalls in designing heterogeneous catalysts with molecular precision. Nat Chem 2025;17:318–24.
[4] Moriau L, Smiljanić M, Lončar A, Hodnik N. Supported iridium-based oxygen evolution reaction electrocatalysts-recent developments. ChemCatChem 2022;14:e202200586.
[5] McCrory CCL, Jung S, Peters JC, Jaramillo TF. Benchmarking heterogeneous electrocatalysts for the oxygen evolution reaction. J Am Chem Soc 2013;135:19677–87.
[6] Kim Y-T, Lopes PP, Park S-A, Lee AY, Lim J, Lee H, et al. Balancing activity,

stability and conductivity of nanoporous core-shell iridium/iridium oxide oxygen evolution catalysts. Nat Commun 2017;8:1449.
[7] Geiger S, Kasian O, Ledendecker M, Pizzutilo E, Mingers AM, Fu WT, et al. The stability number as a metric for electrocatalyst stability benchmarking. Nat Catal 2018;1:508–15.
[8] Yang Z, Wu X, Cai L, Yun J, Zhang J, Liang X, et al. Porous antimony tin oxide with particle assembly structure as an IrO_2 support for efficient oxygen evolution reaction in PEM water electrolysis. ACS Appl Mater Interfaces 2025;17:23348–56.
[9] Lim J, Kim M, Jeon SS, Lee JW, Kim H-E, Kim G, et al. Advanced high current density activity in proton exchange membrane water electrolysis with mass transport enhanced Ir nanodendrites. Energy 2025;333:137439.
[10] Li S, Xiao L, Li H, Li L, Tian T, Wang Y, et al. Preparation and electrocatalytic performance of a nitrogen-doped TiO_2-based self-supported electrode. Energy Fuels 2025;39:20584–92.
[11] She L, Zhao G, Ma T, Chen J, Sun W, Pan H. On the durability of iridium-based electrocatalysts toward the oxygen evolution reaction under acid environment. Adv Funct Mater 2022;32:2108465.
[12] Hodges A, Hoang AL, Tsekouras G, Wagner K, Lee CY, Swiegers GF, et al. A high-performance capillary-fed electrolysis cell promises more cost-competitive renewable hydrogen. Nat Commun 2022;13:1304.
[13] Ge X, Xu K, Liu Z, Liang X, Liang J, Li Y, et al. Lattice defects coupled with support modification enable a BiNi-Co_3O_4/CP catalyst for high-efficiency acidic oxygen evolution reaction. ACS Appl Mater Interfaces 2025;17:58279–87.
[14] Pei Z, Zhang H, Wu ZP, Lu XF, Luan D. Atomically dispersed Ni activates adjacent Ce sites for enhanced electrocatalytic oxygen evolution activity. Sci Adv 2023;9. eadh1320.
[15] Feng B, Chen J, Yang Y, Yang M, Wang H, Zhong C, et al. Facile synthesis of nanosized spinel high entropy oxide $(FeCoNiCrMn)_3O_4$ for efficient oxygen evolution reaction. J Materiomics 2024;10:919–27.
[16] Gil-Sepulcre M, Llobet A. Molecular water oxidation catalysts based on first-row transition metal complexes. Nat Catal 2022;5:79–82.
[17] Ebejer N, Schnippering M, Colburn AW, Edwards MA, Unwin PR. Localized high resolution electrochemistry and multifunctional imaging: scanning electrochemical cell microscopy. Anal Chem 2010;82:9141–5.
[18] Gaudin LF, Wright IR, Harris-Lee TR, Jayamaha G, Kang M, Bentley CL. Five years of scanning electrochemical cell microscopy (SECCM): new insights and innovations. Nanoscale 2024;16:12345–67.
[19] Bentley CL. Scanning electrochemical cell microscopy for the study of (nano)particle electrochemistry: from the sub-particle to ensemble level. Electrochem Sci Adv 2022;2:e2100081.
[20] Jayamaha G, Maleki M, Bentley CL, Kang M. Practical guidelines for the use of scanning electrochemical cell microscopy (SECCM). Analyst 2024;149:2542.
[21] Sherrell PC, Iesalnieks M, Ehrnst Y, Rezk AR, Šutka A. Electrocatalysis for green(er) chemistry: limitations and opportunities with traditional and emerging characterization methods for tangible societal impact. Adv Energy Sustain Res 2024;5:2400008.
[22] Tsujiguchi T, Kawabe Y, Jeong S, Ohto T, Kukunuri S, Kuramochi H, et al. Acceleration of electrochemical CO_2 reduction to formate at the Sn/Reduced graphene oxide interface. ACS Catal 2021;11:3310–8.
[23] Takahashi Y, Kobayashi Y, Wang Z, Ito Y, Ota M, Ida H, et al. High-resolution electrochemical mapping of the hydrogen evolution reaction on transition-metal dichalcogenide nanosheets. Angew Chem Int Ed 2020;59:3629–36.
[24] Mefford JT, Akbashev AR, Kang M, Bentley CL, Gent WE, Deng HD, et al. Correlative operando microscopy of oxygen evolution electrocatalysts. Nature 2021;593:67–73.
[25] Li M, Ye K-H, Qiu W, Wang Y, Ren H. Heterogeneity between and within single hematite nanorods as electrocatalysts for oxygen evolution reaction. J Am Chem Soc 2022;144:5247–52.
[26] Al-Zuraiji SM, Benkó T, Illés L, Németh M, Frey K, Sulyok A, et al. Utilization of hydrophobic ligands for water-insoluble Fe(II) water oxidation catalysts – immobilization and characterization. J Catal 2020;381:615–25.